International Journal for Housing Science and Its Applications

Publish September 9, 2025. Volume 47, Issue 1 Pages 337-348

https://doi.org/10.70517/ijhsa47127

Hybrid neural network for real-time arrhythmia detection and blood pressure trend prediction in wearable monitoring systems

Wenshan Chen[1,*], Peisong Ye[2] and Xiuling Jiang[3]

[1] School of Medical Technology and Engineering, Fujian Health College, Fuzhou, Fujian, 350101, China

[2] Fujian Provincial Hospital, Fuzhou University, Fuzhou, Fujian, 350001, China

[3] Department of Social Sports, Fujian Sports Vocational Education and Technical College, Fuzhou, Fujian, 350003, China

Corresponding authors: (e-mail: wschen2026@126.com).

Abstract This paper designs an overall scheme for a wearable multi-sensor physiological monitoring system, which monitors physiological parameters such as electrocardiogram signals and blood pressure. It combines CNN, LSTM, and MHA and optimizes them using the NRBO algorithm to construct a CNN-LSTM-MHA hybrid neural network model. The performance of this model in heart rate monitoring and blood pressure prediction is evaluated through experiments. In terms of heart rate detection and blood pressure prediction, the CNN-LSTM-MHA model demonstrates the best overall performance and exhibits superior robustness.

Index Terms hybrid neural network, CNN-LSTM-MHA, wearable monitoring system, physiological parameters

I. Introduction

As unhealthy lifestyles such as smoking, poor diet, and lack of exercise become increasingly prevalent among the population, the risk factors associated with cardiovascular disease pose a threat to public health, with mortality rates from cardiovascular disease showing an upward trend year by year [1]-[3]. Arrhythmia is a common heart condition caused by disorders in the cardiac conduction system or myocardial electrophysiological function. Based on their underlying mechanisms and the rate of heartbeat, arrhythmias can be classified into multiple types. Among the seven common types of arrhythmias, not all require treatment; however, malignant arrhythmias can lead to sudden cardiac death within minutes and are the most common trigger for sudden cardiac death, which is one of the primary causes of death among cardiovascular disease patients [4]-[8]. Additionally, the normal blood pressure range for healthy individuals is a systolic pressure of 90-139 mmHg and a diastolic pressure of 60-89 mmHg. If blood pressure is measured three times on non-consecutive days and the systolic pressure is >140 mmHg or the diastolic pressure is >90 mmHg, hypertension can be diagnosed. Hypertension is a major risk factor for cardiovascular disease, exerting sustained pressure on the cardiovascular system and leading to structural and functional changes in the heart and blood vessels, thereby increasing the risk of cardiovascular diseases such as coronary heart disease, myocardial infarction, and heart failure [9]-[11]. Given the high incidence, acute nature, and heavy rehabilitation burden of cardiovascular diseases, monitoring arrhythmias and blood pressure and implementing effective prevention and treatment measures are crucial. This not only helps reduce the incidence of sudden cardiac death but also slows the progression of cardiovascular diseases [12]-[14].

Electrocardiography (ECG) is an important diagnostic tool for cardiovascular diseases. Compared with other clinical examinations, it has the advantages of being easy to operate, low cost, reusable, and non-invasive. However, traditional ECG examination equipment is usually bulky, complex in structure, and expensive, which limits its use to specific locations such as hospitals. This prevents continuous and effective ECG monitoring, leading to occasional abnormal symptoms being missed, and diagnosed diseases may also be difficult to treat promptly due to the irregular nature of their onset cycles [15]-[19]. Additionally, ECG testing requires further analysis by a physician, prolonging the diagnostic process.

With the continuous maturation of IoT and AI technologies, researchers have begun exploring the design of wearable monitoring devices. These devices can promptly issue alerts to help users identify potential health risks and take corresponding treatment measures, or users can independently view relevant physiological data to assess their health status, thereby achieving disease prevention. Healthcare professionals can use the physiological data displayed by the devices to assist in diagnosis and treatment, significantly improving diagnostic efficiency and accuracy [20]-[24]. Therefore, wearable monitoring devices play a significant role in the prevention and treatment of cardiovascular diseases. For example, Hiraoka et al. [25] used an Apple Watch equipped with a photoplethysmography (PPG) sensor to monitor postoperative atrial fibrillation in cardiac surgery patients. Combined with ECG data, these measurements were analyzed using machine learning, achieving a detection accuracy of 94.16%. With the continuous advancement of “Internet+healthcare,” the integration of these technologies will continue to create new application scenarios and business models, thereby driving the formation of new smart healthcare service models. The future trend in wearable monitoring systems is to combine IoT and AI technologies with sensor devices to transmit patients' physiological data in real time to cloud platforms, enabling doctors to conduct remote monitoring and diagnosis through these platforms and provide personalized healthcare services [26]-[28]. Kaisti et al. [29] developed a low-cost flexible wearable wristband for continuous cardiovascular health monitoring, achieving an accuracy rate and sensitivity of 100% and 99.1%, respectively, for heart rate monitoring, enabling effective remote and personalized cardiovascular disease care.

In research on arrhythmia detection, Sraitih et al. [30] compared the performance of three machine learning techniques—support vector machines (SVM), k-nearest neighbors (KNN), and random forests (RF)—and their three hybrid methods in constructing an ECG arrhythmia automatic detection system, with SVM achieving the best accuracy of 83%. Ullah et al. [31] constructed one-dimensional and two-dimensional convolutional neural networks (CNNs) for ECG arrhythmia detection, achieving classification accuracy rates of 97.38% and 99.02%, respectively. Mahmud et al. [32] shared an efficient deep CNN architecture implemented with deep convolutional layers and temporal convolutions for automatically detecting and classifying arrhythmias from denoised ECG beats, outperforming traditional detection methods. Liu et al. [33] designed a new autoencoder using long short-term memory (LSTM) networks for arrhythmia classification, eliminating the need for preprocessing ECG signal data and addressing the gradient vanishing issue in traditional CNNs. Zeng et al. [34] proposed an ECG signal decomposition method using adjustable Q-factor wavelet transform and complete set empirical mode decomposition, followed by input into a hybrid neural network model combining 1D CNN and LSTM for arrhythmia detection, achieving a 96% accuracy rate even when detecting seventeen types of heartbeats. Kuila et al. [35] combined LSTM with differential evaluation algorithms to correct imbalanced ECG heartbeat data and optimize focus loss, achieving an accuracy of 98.23% in ECG arrhythmia detection. Xu et al. [36] integrated a one-dimensional CNN with a gated recurrent unit network to establish an automatic arrhythmia detection model, achieving detection accuracy and sensitivity of 99.45% and 98.35%, respectively, on ECG signal data. He et al. [37] addressed the challenges of heartbeat recognition and the limitations of considering frequency patterns and heart rhythm in arrhythmia detection based on feature engineering and deep learning. They designed an ECG arrhythmia detection method supported by the Internet of Things, combining feature engineering-based dynamic heartbeat classification and multi-channel heartbeat convolutional neural networks.

In blood pressure prediction research, Zhang et al. [38] used a support vector machine regression algorithm for blood pressure prediction, enabling continuous blood pressure measurement. Compared to linear regression and backpropagation neural network algorithms, this method achieved higher accuracy and effectiveness in blood pressure prediction. Rong and Li [39] reported a multi-type feature fusion neural network model based on CNN and bidirectional LSTM for blood pressure prediction under PPG signals, which not only reduced computational complexity but also improved accuracy. Liu et al. [40] utilized blood pressure and wearable features to generate causal graphs, combined with spatio-temporal graph neural networks, to obtain more precise continuous blood pressure prediction results. Koshimizu et al. [41] proposed a deep neural network-based method for predicting blood pressure fluctuations, capable of forecasting blood pressure changes over the next four weeks, though it is more suitable for individuals with significant blood pressure variability. Ali and Atef [42] utilized PPG data in a classification-regression hybrid model combining LSTM and artificial neural networks to predict blood pressure, thereby enhancing prediction accuracy while balancing performance and efficiency. Zhang et al. [43] introduced gradient-boosted decision trees to analyze PPG and ECG signal data, enabling individual blood pressure prediction, though the prediction accuracy for systolic and diastolic blood pressure did not reach 80%. Kamanditya et al. [44] designed a architecture integrating convolutional and LSTM layers with PPG and ECG signals to extract signal features, improving blood pressure prediction accuracy while simplifying the design architecture. Zhang et al. [45] applied PPG and ECG signal data, using the SE block (Squeeze-and-Excitation Block) to enhance feature learning capabilities, and developed a one-dimensional compression and excitation network for blood pressure prediction with the assistance of the LSTM algorithm. This method achieved prediction accuracy rates of 94% and 91% based on systolic and diastolic blood pressure, respectively.

The paper first monitors physiological signals such as ECG and blood pressure from wearers of wearable monitoring devices. After analyzing the application scenarios and requirements, it designs the overall structure and hardware/software solutions for the wearable monitoring system, as well as the upper-level node design scheme. It integrates CNN, LSTM, and MHA, and uses the NRBO optimization algorithm to optimize the parameters of the CNN-LSTM-MHA fusion model, thereby improving the accuracy of arrhythmia detection and blood pressure trend prediction, as well as the model's performance. This paper designs relevant experiments to collect and evaluate physiological signals from participants. The CNN-LSTM-MHA model is compared with other monitoring methods to evaluate its performance in arrhythmia detection and blood pressure prediction.

II. Overall design of a wearable multi-sensor physiological monitoring system

II. A. Physiological parameter monitoring plan

II. A. 1) Electrocardiogram signal monitoring

Although modern ECG acquisition systems have achieved high precision and stability, the inherent weak amplitude of ECG signals (typically ranging from 0.05 to 5 mV) inevitably leads to various noise interferences during actual acquisition. The raw ECG signal, after being pre-amplified, undergoes analog-to-digital conversion (ADC). The resolution of the ADC (typically 12 to 24 bits) and the sampling rate (typically 500 Hz to 1 kHz) determine the precision and temporal resolution of the digital signal. The digitized ECG signal can then be further processed using a computer or specialized equipment.

To ensure signal quality, noise suppression must be addressed at both the hardware and software levels. In hardware design, high common-mode rejection ratio preamplifiers, reasonable circuit design, and proper grounding measures should be adopted; in software processing, the ability to analyze high- and low-frequency noise in both the time domain and frequency domain is required, enabling the ECG signal to be decomposed into high- and low-frequency signal components at different scales. This enables key steps such as noise suppression, baseline drift correction, and QRS complex detection.

First, a discrete wavelet transform with dynamic selection of wavelet bases is used to decompose the electrocardiogram signal $x[n]$ into the Jth-level approximation coefficients $A_j[n]$ and detail coefficients $D_j[n]$, satisfying:

$$A_j[n] = \sum_k h_{opt} h[k] A_{j+1}[2n-k] \tag{1}$$

$$D_j[n] = \sum_k g_{opt} g[k] A_{j+1}[2n-k] \tag{2}$$

Among these, $A_j[n]$ represents the approximation coefficient of the Jth layer, indicating the low-frequency components of the signal, $D_j[n]$ represents the detail coefficient of the Jth layer, indicating the high-frequency components of the signal, h_{opt}, g_{opt} represent the low-pass and high-pass filter coefficients corresponding to the optimal wavelet basis, respectively, $h[k]$ represents the low-pass filter coefficients used to extract low-frequency information, $g[k]$ represents the high-pass filter coefficients used to extract high-frequency information, and A_{j+1} represents the approximation coefficients of the (J+1)th layer.

The threshold denoising process applies kurtosis weighting to traditional soft threshold processing, which improves the processing accuracy of detail coefficients. The approximation component $A_j[n]$ of the Jth layer captures low-frequency baseline drift, and the detail components $D_j[n]$ of each layer correspond to different frequency bands (such as high-frequency noise, QRS band, etc.).

First, the signal is layered through cascaded decomposition to separate different frequency band components. Then, adaptive thresholds are applied to the detail coefficients $D_j[n]$ of each layer to suppress high-frequency noise and retain useful QRS wave information:

$$D_j[n] = \begin{cases} sign(D_j[n])(|D_j[n]| - T_j), & |D_j[n]| > T_j \\ 0 & |D_j[n]| > T_j \end{cases} \tag{3}$$

$$T_j = \sigma_j \sqrt{2lnN}(1 + \frac{kurt(D_j)}{10}) \tag{4}$$

$$\sigma_j = \frac{median|D_j|}{0.6745} \tag{5}$$

Among these, T_j represents the threshold of the Jth layer, $|D_j[n]|$ represents the absolute value of the detail coefficient, $kurt(D_j)$ represents the kurtosis factor, which enhances robustness against non-Gaussian noise, σ_j represents the estimated standard deviation of the detail coefficient noise for the Jth layer, N represents the signal length (number of sampling points), and $median|D_j|$ represents the median of the absolute value of the detail coefficient.

The baseline drift component is estimated using the approximation coefficient of the highest layer, and subtracted from the signal to achieve baseline correction:

$$Baseline[n] = \sum_k h_{rec}[k] A_j(\frac{n-k}{2^j}) \tag{6}$$

$$x_{corr}[n] = x[n] - Baseline[n] \tag{7}$$

Among them, $h_{rec}[k]$ represents the low-pass filter used for reconstruction, Baseline[n] represents the estimated baseline drift signal (from the highest-level approximation coefficient A_j), and $x_{corr}[n]$ represents the corrected signal.

For QRS complex detection, the kth layer detail coefficient with the best match to the QRS frequency band is selected. First, its energy envelope is calculated, and then an adaptive threshold is set as shown in Equation (8):

$$E[n]=\frac{1}{W}\sum_{i=0}^{W-1}(D_k^{'}[n-i])^2 \tag{8}$$

MATLAB was used to simulate the ECG preprocessing algorithm and obtain the comparison results before and after preprocessing. The figure shows that the original ECG signal was significantly affected by baseline drift and high-frequency noise interference. After adaptive wavelet threshold denoising, the high-frequency noise was effectively suppressed while retaining the main features of the ECG signal. The baseline drift correction process accurately estimated the low-frequency drift component, and the corrected signal had a stable baseline.

II. A. 2) Blood pressure monitoring

(1) PPG signal

Photoplethysmography (PPG) is a biological signal that uses optical technology to measure changes in blood volume [46]. PPG sensors typically consist of light-emitting diodes (LEDs) and light-sensitive detectors (such as photodiodes). The LED emits light of a specific wavelength (usually red or infrared) onto the skin surface, which penetrates through the epidermis, dermis, and other skin tissue layers. Due to the specific absorption characteristics of blood, when the heart beats, the blood volume in the blood vessels undergoes periodic changes, leading to corresponding changes in the absorption and reflection of light in the skin tissue.

(2) Principle of photoplethysmography for blood pressure measurement

Blood pressure monitoring based on PPG primarily relies on the extraction and analysis of pulse wave characteristic parameters. Among these, pulse wave transmission time (PWTT) serves as an important indicator reflecting the functional state of the cardiovascular system and exhibits a good correlation with blood pressure changes. By combining electrocardiogram (ECG) and PPG signals, PWTT can be precisely calculated, enabling continuous, non-invasive blood pressure monitoring.

When blood pressure increases, the pressure on arterial walls also increases. Prolonged exposure to high pressure can lead to structural changes in arterial walls, making them harder (i.e., arterial sclerosis). This increased stiffness directly accelerates the propagation speed of pulse waves in arteries, thereby shortening the pulse wave transmission time. When blood pressure is low, the pressure on arterial walls is reduced, and arteries maintain better elasticity, slowing the propagation speed of pulse waves and resulting in a longer pulse wave transmission time. The relationship between pulse wave velocity (PWV) and pulse wave transmission time (PWTT) can be expressed as:

$$\varphi=\alpha\cdot\overline{E}+\beta std(E) \tag{9}$$

In this context, $E[n]$ represents the sliding energy envelope of the detail coefficient D_k, W denotes the window length, φ is the adaptive threshold used for detecting the QRS wave, α,β are weighting coefficients, and $\overline{E},std(E)$ represent the mean and standard deviation of the energy envelope, respectively.

When $E[n]>\varphi$ and it is a local maximum, the R wave candidate is marked, and the R peak is precisely located within the small interval of x_{corr}. Finally, the processed coefficient set $\{A_j,D_j^{'}\cdots D_1^{'}\}$ is reconstructed into a denoised and drift-corrected signal via inverse wavelet transform:

$$x_{denoise}[n]=\sum_k h_{rec}[k]A_j\left(\frac{n-k}{2^j}\right)+\sum_{j=1}^{j}\sum_k g_{rec}[k]D_j^{'}\left(\frac{n-k}{2^j}\right) \tag{10}$$

Among these, $h_{rec}[k]g_{rec}[k]$ represents the reconstruction filter bank, $D_j^{'}$ represents the detail coefficients after threshold processing, 2^j represents the sampling factor for layer J, and $x_{denoise}[n]$ represents the clean ECG signal reconstructed from the denoised coefficients.

Heart rate measurement is based on the detection of QRS complexes in the ECG. A QRS complex represents a single contraction of the heart. By detecting the frequency of these QRS complexes and calculating the time interval between two consecutive R waves (RR interval), the heart rate can be determined, as shown in Equation (11):

$$\text{Heart rate(BPM)}=\frac{60}{\text{R-R Interval (seconds)}} \tag{11}$$

$$PWV=\frac{L}{PWTT} \tag{12}$$

Among them, PWV represents the pulse wave velocity, which indicates the speed at which waves propagate through the arteries, L represents the distance traveled by the pulse wave, and $PWTT$ represents the pulse wave transmission time.

Thomas Young proposed a formula for the propagation of wave velocity in an ideal fluid within an elastic pipe:

$$C = \sqrt{\frac{Eh}{\rho D}} \tag{13}$$

In this formula, E, h represent the Young's modulus and wall thickness of the arterial vessel, respectively, ρ represents the density of blood, and D represents the equilibrium inner diameter of the arterial vessel.

The relationship between arterial blood pressure and the elastic modulus of the arterial vessel is shown in Formula (14):

$$E = E_0 e^{rP} \tag{14}$$

In this equation, $E_0 E$ represents the initial elastic modulus of the blood vessel and the elastic modulus of the vessel wall, respectively, r represents a constant characteristic of the blood vessel, typically ranging from 0.016 to 0.018 ($mmHg^{-1}$), and P represents the blood pressure value.

Substituting equations (9) and (11) into equation (10) yields:

$$P = \frac{1}{r}\left[\ln\left(\frac{\rho D L^2}{h E_0}\right) - 2\ln(PWTT)\right] \tag{15}$$

Assuming that changes in blood pressure cause negligible changes in the diameter of the artery and the thickness of the arterial wall, equation (12) can be transformed to:

$$\frac{dP}{dT} = -\frac{2}{r \cdot PWTT} \tag{16}$$

Based on the theory of vascular elasticity mechanics and fluid dynamics principles, combined with the derivation of equations (9) to (12), the inverse relationship between blood pressure and pulse wave transmission time shown in equation (13) is derived. However, under actual physiological conditions, the two exhibit complex nonlinear characteristics. This study employs a polynomial fitting method to establish a more precise mapping model, representing blood pressure P as a polynomial function of PWTT: $P = a_0 PWTT^0 + a_1 PWTT^1 + a_2 PWTT^2 + ... + a_m PWTT^m$ where $a_0 a_0 ... a_0$ are fitting coefficients determined by the least squares method. This method effectively approximates the nonlinear relationship between blood pressure and PWTT, thereby improving the accuracy of blood pressure estimation.

II. B. Application Scenarios and Requirements Analysis

This paper designs a wearable multi-sensor physiological parameter monitoring system capable of measuring skin temperature signals, electrocardiogram signals, and pulse wave signals on the human body surface. It enables real-time continuous monitoring of physiological parameters such as body temperature, blood pressure, blood oxygen saturation, and pulse rate. The obtained data can be applied not only to personal daily health monitoring but also to disease auxiliary diagnosis, drug efficacy tracking, and related scientific research.

II. C. Overall System Structure and Hardware/Software Design

II. C. 1) Overall System Structure Design

The specific functions of this system at each layer are as follows:

(1) At the sensor layer: This system uses negative temperature coefficient (NTC) thermistors to collect human skin surface temperature signals; fabric electrodes to collect ECG signals; photodiodes (PD) to collect PPG signals; and inertial measurement units (IMU) to collect ACC signals.

(2) At the measurement level: The temperature information contained in the thermistor's resistance is converted into a voltage signal across the thermistor through a voltage divider circuit structure that connects it in series with a reference resistor, and then acquired via an analog-to-digital converter (ADC). The voltage signals collected by the fabric electrodes are converted into ECG signals through an analog front-end circuit composed of an instrumentation amplifier circuit, hardware filter circuit, and ADC. For PPG signal measurement, photodiodes receive light signals transmitted or reflected from human skin tissue to generate pulse wave signals; ACC signals are measured using an inertial measurement unit based on Newton's second law.

(3) At the processing level: Voltage signals are input into a temperature-voltage conversion formula fitted from a large amount of experimental data to obtain temperature values; ACC signals synchronously collected with PPG signals are used to provide motion artifact information, i.e., to determine the subject's motion state during measurement, then the PPG data is filtered based on the motion state, and the synchronously collected ECG data undergoes the same processing. The processed

PPG data is then input into a pulse rate calculation program to obtain the pulse rate value, input into a blood oxygen saturation calculation program to obtain the blood oxygen value, and input together with the processed ECG data into a feature extraction program to obtain a feature set for blood pressure prediction. Finally, the feature set is input into a trained machine learning model to obtain the blood pressure prediction result.

(4) Transmission, display, and storage: This system uses low-energy Bluetooth (BLE) as the wireless communication method between devices. The dongle serves as the host, while the ECG acquisition device, temperature acquisition device, and pulse wave acquisition device serve as the clients. After the host receives data from the clients, it parses and packages the data before sending it to the PC via a serial port. On the PC side, a host software application is developed using the Python graphical user interface development library PyQt5. This software can display measurement results for body temperature, blood pressure, blood oxygen saturation, and pulse rate on the main interface in either numerical or waveform format. Additionally, the software can store various physiological parameters and raw signals in formats such as txt and xlsx.

II. C. 2) Overall System Hardware and Software Design

The system consists of hardware components including an electrocardiogram (ECG) acquisition device, a pulse wave acquisition device, a skin temperature acquisition device, a data reception device, and a PC. The software components include programs for each signal acquisition device, a program for the data reception device, and a host computer program. From the perspective of the physiological parameters measured, temperature measurement is performed by a temperature acquisition hardware device combined with its accompanying embedded program. Pulse rate and blood oxygen measurement is performed by a pulse wave acquisition hardware device combined with its accompanying embedded program. Blood pressure measurement results are output by the blood pressure monitoring software module in the host computer software, with the raw signal information used by this module provided by the electrocardiogram acquisition device and pulse wave acquisition device.

II. D. Host Node Design Plan

The design scheme for the host computer node is shown in Figure 1. The host computer node consists of two parts: a Bluetooth dongle that receives and forwards data, and a PC equipped with host computer software. In Bluetooth transmission, the dongle acts as the host, receiving data sent from the temperature acquisition module, ECG acquisition module, and pulse wave acquisition module. It then sends the received data to the PC via a serial port using DMA technology in a specific data format. In addition to forwarding data, the host computer sends low-power commands to the dongle via serial port interrupts. After parsing the received commands, the dongle sends these low-power commands to the specified data acquisition devices via Bluetooth using write feature values.

For the host computer software on the PC, after configuring the corresponding serial port, Subthread 1 stores the data received via the serial port into RAM and parses it. For the three pre-calculated physiological parameters—body temperature, pulse rate, and blood oxygen saturation—the main thread directly displays them on the main interface in the form of waveform charts and numerical values. For the two sets of synchronized data (one set consisting of ECG and acceleration data, and the other set consisting of single-channel pulse wave and acceleration data), subthread 2 calculates blood pressure values through a series of steps including data preprocessing, feature extraction, and blood pressure prediction, and displays the results in two formats on the main interface via the main thread.

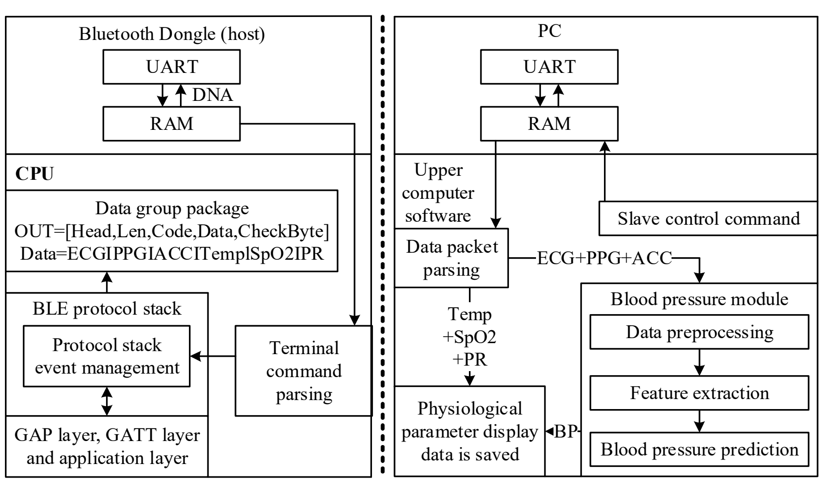

Figure 1: The first machine node design case

III. Classification prediction model based on hybrid neural networks

This model combines a convolutional neural network (CNN), a long short-term memory network (LSTM), and a multi-head attention mechanism (MHA), and uses the Newton-Raphson optimization algorithm (NRBO) for parameter optimization [47]. The CNN-LSTM-MHA model can extract features from electrocardiogram and blood pressure signals in terms of time series, spatial, and feature relationships, significantly improving classification accuracy and model performance.

Overfitting is a common issue in machine learning and deep learning, referring to a situation where a model performs well on training data but poorly on test data or unseen data. Solutions include increasing training data, simplifying the model, regularization, and early stopping. To mitigate overfitting, this design employs Dropout regularization, batch normalization, and the Adam optimizer to optimize the model.

(1) Dropout Regularization

Dropout is a regularization method used in neural network training to mitigate overfitting. Its core idea is to randomly disable some neurons during training, forcing the network to rely on different subsets of neurons for training in each iteration. This method effectively reduces the model's dependence on specific neurons, enabling the network to learn a wider range of features and thereby enhance its generalization ability when handling unseen data, ultimately improving its performance on new data.

During training, each neuron is retained or discarded with a certain probability p. The retention probability is p, and the dropout probability is $1-p$. For the neurons in the i th layer, generate a Bernoulli distribution random vector r with the same dimension, where each element has a probability of p to be 1 and a probability of $1-p$ to be 0. Multiply this random vector by the neuron output element by element:

$$h' = r \odot h \tag{17}$$

Where h is the output of the i th layer neuron, and $\odot$ denotes element-wise multiplication.

In the testing phase, to ensure consistency of the output, the neuron output needs to be scaled by multiplying the retention probability p by the output:

$$h = p \cdot h' \tag{18}$$

(2) Batch Normalization

is a method of normalizing neural networks. It normalizes the input data before the activation function in each layer. This makes the input distribution in each layer more stable, thereby accelerating training and improving model performance. Since the mean and variance of each mini-batch are random during training, Batch Normalization has a certain regularization effect, which can reduce dependence on Dropout. The calculation steps for Batch Normalization are as follows.

Calculate the mean and variance of the mini-batch. For layer l, the mini-batch $B = \{x_1, x_2, \ldots, x_m\}$, where m is the size of the mini-batch:

$$\mu_g = \frac{1}{m}\sum_{i=1}^{m} x_i \tag{19}$$

$$\sigma_B^2 = \frac{1}{m}\sum_{i=1}^{m}(x_i - \mu_B)^2 \tag{20}$$

Standardize the input data so that its mean is 0 and its variance is 1.

$$\hat{x}_i = \frac{x_i - \mu_3}{\sqrt{\sigma_B^2 + \epsilon}} \tag{21}$$

Here, ϵ is a small constant used to avoid division by zero errors.

Learnable parameters γ and β are introduced so that the standardized data has different means and variances.

$$y_i = \gamma \hat{x}_i + \beta \tag{22}$$

(3) Adam Optimization Algorithm

Adam is an adaptive learning rate optimization algorithm [48] that combines the advantages of momentum and RMSProp optimization methods and is suitable for handling large-scale data and high-dimensional parameter optimization problems. Adam adapts the learning rate for each parameter by calculating the first-order moment estimate and second-order moment estimate of the gradient, enabling it to quickly find optimal parameters during training and significantly accelerate training speed.

Detailed application process of the Adam algorithm:

(1) Initialization

Initialize some variables and hyperparameters. The initial parameters of the model are θ_0, the initial value of the momentum term is $m_0 = 0$, the initial value of the root mean square propagation term is $v_0 = 0$, the current iteration count is $t = 0$, and the learning rate is typically set to $\alpha = 0.001$ by default. the decay rate for the first-order moment estimate is typically set to $\beta_1 = 0.9$ by default, the decay rate for the second-order moment estimate is typically set to $\beta_2 = 0.999$ by default, and the small constant to prevent division by zero is typically set to $\epsilon = 10^{-8}$ by default.

(2) Calculate the gradient

At each time step t, calculate the gradient of the loss function $L(\theta_{t-1})$ with respect to the current parameters θ_{t-1}:

$$g_t = \nabla \theta_{t-1} L(\theta_{t-1}) \tag{23}$$

(3) Update the first-order and second-order moment estimates.

Update the first-order moment estimate m_i and the second-order moment estimate v_i:

$$m_t = \beta_1 m_{t-1} + (1-\beta_1) g_t \tag{24}$$

$$v_t = \beta_2 v_{t-1} + (1-\beta_2) g_t^2 \tag{25}$$

(4) Perform bias correction.

Perform bias correction on the first-order and second-order moment estimates to reduce the bias at the initial moment:

$$\hat{m}_t = \frac{m_t}{1-\beta_1} \tag{26}$$

$$\hat{v}_t = \frac{v_t}{1-\beta_2'} \tag{27}$$

(5) Update parameters

Use the corrected moment estimates to update the parameters:

$$\theta_t = \theta_{t-1} - \alpha \frac{\hat{m}_t}{\sqrt{\hat{v}_t} + \epsilon} \tag{28}$$

IV. Experimental analysis

IV. A. Physiological Signal Acquisition and Analysis

This study recruited five college students as subjects (designated A–E), including three males and two females, aged 18–22 years. The test values were the average of five measurements taken from each subject, and the reference values were the measurements from the Mindray uMEC7 monitor.

The subjects' blood oxygen saturation, heart rate, and blood pressure data are shown in Table 1. As shown in Table 1, the blood oxygen saturation values of the 5 subjects ranged from 97.6% to 98.5%, heart rate from 66.3 to 76.1 beats per minute, systolic blood pressure from 109.2 to 138.6 mmHg, and diastolic blood pressure from 65.5 to 86.7 mmHg, all within the normal range for human distribution. Compared with the calibrated values of physiological parameters measured by the Mindray uMEC7 monitor, the maximum relative errors of blood oxygen saturation, heart rate, systolic blood pressure, and diastolic blood pressure measured by this monitoring system were 1.34%, 0.80%, 0.50%, and 1.87%, respectively. All test errors were within 2.00%, validating the effectiveness of this system in measuring blood oxygen saturation, heart rate, and blood pressure data.

This study analyzed the individual differences in the physiological data shown in Table 1. The results showed that the P-values of the t-test analysis of the physiological parameter measurements of individual subjects were all less than 0.05, indicating that there were significant differences in the physiological parameter values of individual subjects. On the one hand, this was due to differences in the physiological parameters of subjects of different genders. On the other hand, it was because the psychological and physical states of the subjects during the data collection process were different, leading to differences in their physiological parameter values.

Table 1: Blood oxygen saturation, heart rate and blood pressure data of the subjects

		A	B	C	D	E
Blood oxygen saturation /%	Test value	98.5	98.1	98.3	97.8	97.6
	Nominal value	97.2	98.8	98.4	97.8	97.9
	Relative error	1.34%	0.71%	0.10%	0.00%	0.31%
Heart rate /min	Test value	75.2	66.3	76.1	65.2	72.4
	Nominal value	74.6	66.1	76.3	64.8	72.5
	Relative error	0.80%	0.30%	0.26%	0.62%	0.14%
Systolic pressure /mmHg	Test value	138.6	109.2	136.2	110.3	125.5
	Nominal value	139.3	109.6	136.5	110.7	125.0
	Relative error	0.50%	0.36%	0.22%	0.36%	0.40%
Diastolic pressure /mmHg	Test value	85.3	86.7	78.4	65.5	75.6
	Nominal value	84.6	87.2	77.8	65.2	74.2
	Relative error	0.83%	0.57%	0.77%	0.46%	1.87%

IV. B. Quality Assessment Performance Comparison

IV. B. 1) Comparative analysis of heart rate detection results

To evaluate the performance of CNN-LSTM-MHA, it was compared with algorithms based on manual features and mainstream classification task models. The mainstream classification task models compared include ResNet, DenseNet, MobileNetv2, ShuffleNetv2, and DNN for ECG signal classification. We have made every effort to manually tune the hyperparameters of the aforementioned convolutional network models to their optimal levels, and these models were implemented within the same framework as CNN-LSTM-MHA.

The comparison results of the CNN-LSTM-MHA algorithm with other methods on the wearable ECG dataset are shown in Table 2. The results in Table 2 indicate that CNN-LSTM-MHA outperforms handcrafted feature-based algorithms across all listed evaluation metrics. This may be due to the difficulty of handcrafted features in identifying ECG data that contains noise but is of acceptable quality. Additionally, these handcrafted feature-based algorithms were modeled on small-scale public datasets collected in hospitals, making them unsuitable for large-scale wearable ECG signal datasets collected by non-professional operators.

Table 2 also shows that CNN-LSTM-MHA outperforms the carefully constructed lightweight CNN model in all metrics except inference time. CNN-LSTM-MHA achieves an ACC of 95.43%, an AUC of 97.16%, an F1 score of 94.13%, and an MCC of 85.24%. The inference time of CNN-LSTM-MHA in the Android emulator is not the shortest; however, the millisecond-level latency has minimal impact on user experience and still meets the real-time requirements for ECG signal quality assessment on mobile devices. Additionally, compared to a DNN with 10 times more parameters, the AUC of CNN-LSTM-MHA is only 0.29% lower.

Table 2: Comparison between other methods and CNN-LSTM-MHA on wearable ECG dataset

Method	Params (K)	ACC (%)	SEN (%)	SPE (%)	AUC (%)	F1 (%)	MCC (%)	FLOPs (%)	Time (ms)
Moody	-	85.28	55.79	97.45	73.06	57.03	59.23	-	-
SOIs	-	86.16	76.04	88.96	87.99	89.62	60.65	-	-
SOIs+SVM	-	84.35	63.69	88.65	84.02	71.98	64.59	-	-
Orphanidou	-	88.17	88.23	76.64	92.74	85.75	64.49	-	-
DNN	7256.34	90.32	97.18	92.62	97.45	85.82	77.85	-	-
Resnet	78.62	85.16	86.44	94.15	84.58	91.22	78.58	34.52	46
Densenet	83.45	92.24	94.79	94.37	87.35	87.67	81.62	33.69	64
ShuffleNetv2	70.69	91.41	95.07	95.07	90.15	93.51	83.23	31.58	92
MobileNetv2	66.48	93.37	85.15	96.36	95.46	91.91	82.59	33.46	50
Ours	65.03	95.43	87.68	97.07	97.16	94.13	85.24	35.78	75

To comprehensively evaluate CNN-LSTM-MHA, experiments compared its performance against four existing quality assessment methods on the PICC 2011 dataset. Comparisons were also conducted with the convolutional network model described in the previous section. To validate the robustness of the proposed hybrid neural network CNN-LSTM-MHA algorithm and arbitrary lead selection strategy, the same network architecture as the quality assessment models described in the aforementioned experiments was employed. The experiments split the 12-lead ECG signals from the PICC 2011 dataset into 12 single-lead signal samples, assigning quality labels to each lead sample during training. During testing, the overall quality score for the 12-lead ECG signal was obtained by averaging the quality scores of the 12 leads generated by the model under the arbitrary lead strategy. Since the private test set of PICC 2011 is not publicly available, five-fold cross-validation was employed for this experiment.

The performance comparison of the CNN-LSTM-MHA algorithm against other methods on the PICC 2011 dataset is shown in Table 3. The ACC of CNN-LSTM-MHA was slightly lower than that of Algorithm and Algorithm DW, potentially due to differences between proprietary wearable ECG signals and PICC 2011 signals. CNN-LSTM-MHA was optimized using ProxylessNAS on a wearable ECG dataset collected via the Mason-Likar lead system, whereas the PICC 2011 dataset was acquired using the Wilson lead system. Nevertheless, CNN-LSTM-MHA still achieved higher ACC than other algorithms. These results further validate the effectiveness of the proposed method.

CNN-LSTM-MHA achieved an ACC of 94.85%, AUC of 97.23%, F1 score of 94.96%, and MCC of 85.74%, outperforming other lightweight CNNs across all metrics. Moreover, most of these lightweight CNNs still performed well in the quality assessment of the PICC 2011 dataset, demonstrating the robustness of the proposed CNN-LSTM-MHA strategy.

Table 3: The performance of other methods and CNN-LSTM-MHA on PICC 2011 dataset

Method	ACC (%)	SEN (%)	SPE (%)	AUC (%)	F1 (%)	MCC (%)
Pan-tompkins	97.56	-	-	-	-	-
Hamilton	90.82	-	-	-	-	-
Martinez	90.52	90.38	90.18	-	-	-
Lourenco	92.41	89.45	96.84	-	85.22	-
DNN	94.36	85.74	90.66	97.58	94.63	84.56
Resnet	88.79	79.86	94.05	96.41	89.47	73.32
Densenet	92.46	75.42	99.16	96.03	91.57	82.09
ShuffleNetv2	82.84	66.49	85.78	84.66	83.64	52.46
MobileNetv2	90.63	72.45	97.15	95.42	91.74	77.49
Ours	94.85	87.37	96.08	97.23	94.96	85.74

Table 4: Comparison of blood pressure prediction results

Volunteer	Measure method	SBP		DBP		Dm±SD (mmHg)
		Dm (mmHg)	SD (mmHg)	Dm (mmHg)	SD (mmHg)	
Male	Moody	0.62	3.17	0.38	2.05	5±8
	SOIs	0.36	2.59	0.23	1.81	
	SOIs+SVM	0.78	2.45	0.53	2.35	
	Orphanidou	0.45	2.61	0.42	1.86	
	DNN	0.22	3.21	0.33	2.22	
	Resnet	0.41	2.02	0.23	2.92	
	Densenet	0.95	2.71	0.11	2.87	
	ShuffleNetv2	0.43	2.39	0.47	2.63	
	MobileNetv2	0.85	2.16	0.39	2.34	
	Ours	0.09	1.21	0.05	1.47	
Female	Moody	1.62	1.85	1.43	1.89	
	SOIs	1.49	2.32	0.83	2.27	
	SOIs+SVM	1.43	1.97	1.31	2.31	
	Orphanidou	0.61	2.33	0.77	2.32	
	DNN	0.86	2.15	0.55	2.06	
	Resnet	1.66	2.41	1.31	2.15	
	Densenet	0.72	1.99	1.14	2.59	
	ShuffleNetv2	0.87	1.97	1.41	2.52	
	MobileNetv2	1.25	2.26	1.09	2.41	
	Ours	0.67	1.75	0.45	1.79	

IV. B. 2) Comparative analysis of blood pressure prediction results

Further validation of the accuracy of the blood pressure monitoring system proposed in this paper. The comparison of blood pressure prediction results according to AAMI standards is shown in Table 4. This paper calculated two metrics for blood pressure measurement as defined by the Association for the Advancement of Medical Instrumentation (AAMI): mean error (Dm) and standard deviation (SD). As shown in the table, the Dm and SD values of all 10 methods meet AAMI requirements. However, the absolute values of Dm and SD for the CNN-LSTM-MHA blood pressure prediction method proposed in this paper are smaller than those of other blood pressure signal monitoring methods, indicating that the CNN-LSTM-MHA blood pressure prediction method has higher accuracy. The minimum Dm and SD for blood pressure prediction are 0.05 and 1.21 mmHg, respectively, while the minimum Dm and SD for other blood pressure prediction methods are 0.22 and 1.81 mmHg, respectively.

V. Conclusion

This paper investigates hybrid neural networks used in wearable monitoring systems for detecting arrhythmias and predicting blood pressure trends. It proposes a classification prediction model based on hybrid neural networks and evaluates its performance through experiments.

All participants' blood oxygen saturation values, heart rate, systolic blood pressure, and diastolic blood pressure conform to the general distribution patterns of the human body, with testing errors within 2.00%, indicating the validity of the collected data. In terms of heart rhythm detection, the CNN-LSTM-MHA method demonstrated the best overall performance, outperforming other models in all metrics except inference time. Its ACC, AUC, F1, and MCC values were 95.43%, 97.16%, 94.13%, and 85.24%, respectively. On the PICC 2011 dataset, the CNN-LSTM-MHA method achieved ACC, AUC, F1, and MCC values of 94.85%, 97.23%, 94.96%, and 85.74%, respectively, outperforming other lightweight CNN methods and demonstrating better robustness. In terms of blood pressure prediction, the average error and absolute standard error of the CNN-LSTM-MHA blood pressure prediction method in this paper are smaller than those of other blood pressure signal monitoring methods, achieving the highest prediction accuracy.

Funding

This research was supported by the 2024 Fujian Provincial Key Project of Vocational and Lifelong Education (Intelligent Embedded Control Technology); 2024 Fujian Provincial Domestic Visiting Scholar Program for Higher Education Institutions; 2024 Discipline Construction and Teaching Reform Project of Fujian Health College (JG2024112).

References

[1] Shan, Z., Li, Y., Baden, M. Y., Bhupathiraju, S. N., Wang, D. D., Sun, Q. I., ... & Hu, F. B. (2020). Association between healthy eating patterns and risk of cardiovascular disease. JAMA internal medicine, 180(8), 1090-1100.

[2] Gaziano, T. A. (2022). Cardiovascular diseases worldwide. Public Health Approach Cardiovasc. Dis. Prev. Manag, 1, 8-18.

[3] Woodruff, R. C., Tong, X., Khan, S. S., Shah, N. S., Jackson, S. L., Loustalot, F., & Vaughan, A. S. (2024). Trends in cardiovascular disease mortality rates and excess deaths, 2010–2022. American journal of preventive medicine, 66(4), 582-589.

[4] Mandala, S., & Di, T. C. (2017). ECG parameters for malignant ventricular arrhythmias: a comprehensive review. Journal of medical and biological engineering, 37(4), 441-453.

[5] El-Battrawy, I., Lang, S., Ansari, U., Tülümen, E., Schramm, K., Fastner, C., ... & Akin, I. (2018). Prevalence of malignant arrhythmia and sudden cardiac death in takotsubo syndrome and its management. EP Europace, 20(5), 843-850.

[6] Yang, X., Geng, T., Peng, Y., Cui, L., Chen, S., Wang, G., ... & Wu, S. (2024). Associations between cardiac arrhythmias and cardiovascular disease incidence and all-cause mortality: the Kailuan study. BMC public health, 24(1), 3266.

[7] Kingma, J., Simard, C., & Drolet, B. (2023). Overview of cardiac arrhythmias and treatment strategies. Pharmaceuticals, 16(6), 844.

[8] Markwerth, P., Bajanowski, T., Tzimas, I., & Dettmeyer, R. (2021). Sudden cardiac death—update. International journal of legal medicine, 135(2), 483-495.

[9] Frąk, W., Wojtasińska, A., Lisińska, W., Młynarska, E., Franczyk, B., & Rysz, J. (2022). Pathophysiology of cardiovascular diseases: new insights into molecular mechanisms of atherosclerosis, arterial hypertension, and coronary artery disease. Biomedicines, 10(8), 1938.

[10] Hoffmann, F., Fassbender, P., Zander, W., Ulbrich, L., Kuhr, K., Adler, C., ... & Reuter, H. (2022). The hypertension paradox: survival benefit after ST-elevation myocardial infarction in patients with history of hypertension. A prospective cohort-and risk-analysis. Frontiers in Cardiovascular Medicine, 9, 785657.

[11] Díez, J., & Butler, J. (2023). Growing heart failure burden of hypertensive heart disease: a call to action. Hypertension, 80(1), 13-21.

[12] Zhao, D., Liu, J., Wang, M., Zhang, X., & Zhou, M. (2019). Epidemiology of cardiovascular disease in China: current features and implications. Nature Reviews Cardiology, 16(4), 203-212.

[13] Lip, G. Y., Coca, A., Kahan, T., Boriani, G., Manolis, A. S., Olsen, M. H., ... & Reviewers: Dan Gheorghe-Andrei Gorenek Bulent Fauchier Laurent Savelieva Irina Hatala Robert van Gelder Isabelle Brguljan-Hitij Jana Erdine Serap Lovič Dragan Kim Young-Hoon Salinas-Arce Jorge Field Michael. (2017). Hypertension and cardiac arrhythmias: a consensus document from the European Heart Rhythm Association (EHRA) and ESC Council on Hypertension, endorsed by the Heart Rhythm Society (HRS), Asia-pacific heart rhythm society (APHRS) and sociedad latinoamericana de estimulacion Cardiaca y electrofisiologia (SOLEACE). Ep Europace, 19(6), 891-911.

[14] Leong, D. P., Joseph, P. G., McKee, M., Anand, S. S., Teo, K. K., Schwalm, J. D., & Yusuf, S. (2017). Reducing the global burden of cardiovascular disease, part 2: prevention and treatment of cardiovascular disease. Circulation research, 121(6), 695-710.

[15] Bhatia, R. S., & Dorian, P. (2018). Screening for cardiovascular disease risk with electrocardiography. JAMA Internal Medicine, 178(9), 1163-1164.

[16] Xie, L., Li, Z., Zhou, Y., He, Y., & Zhu, J. (2020). Computational diagnostic techniques for electrocardiogram signal analysis. Sensors, 20(21), 6318.

[17] Boriani, G., Palmisano, P., Malavasi, V. L., Fantecchi, E., Vitolo, M., Bonini, N., ... & Freedman, B. (2021). Clinical factors associated with atrial fibrillation detection on single-time point screening using a hand-held single-lead ECG device. Journal of clinical medicine, 10(4), 729.

[18] Waldmann, V., Combes, N., Ladouceur, M., Celermajer, D. S., Iserin, L., Gatzoulis, M. A., ... & Marijon, E. (2020). Understanding electrocardiography in adult patients with congenital heart disease: a review. JAMA cardiology, 5(12), 1435-1444.

[19] Hung, M. Y., Kounis, N. G., Lu, M. Y., & Hu, P. (2020). Myocardial ischemic syndromes, heart failure syndromes, electrocardiographic abnormalities, arrhythmic syndromes and angiographic diagnosis of coronary artery spasm: literature review. International Journal of Medical Sciences, 17(8), 1071.

[20] Mizuno, A., Changolkar, S., & Patel, M. S. (2021). Wearable devices to monitor and reduce the risk of cardiovascular disease: evidence and opportunities. Annual review of medicine, 72(1), 459-471.

[21] Prieto-Avalos, G., Cruz-Ramos, N. A., Alor-Hernandez, G., Sánchez-Cervantes, J. L., Rodriguez-Mazahua, L., & Guarneros-Nolasco, L. R. (2022). Wearable devices for physical monitoring of heart: a review. Biosensors, 12(5), 292.

[22] Healey, J. S., & Wong, J. (2019). Wearable and implantable diagnostic monitors in early assessment of atrial tachyarrhythmia burden. Ep Europace, 21(3), 377-382.

[23] Bayoumy, K., Gaber, M., Elshafeey, A., Mhaimeed, O., Dineen, E. H., Marvel, F. A., ... & Elshazly, M. B. (2021). Smart wearable devices in cardiovascular care: where we are and how to move forward. Nature Reviews Cardiology, 18(8), 581-599.

[24] Obianyo, C., Ezeamii, V. C., Idoko, B., Adeyinka, T., Ejembi, E. V., Idoko, J. E., ... & Ugwu, O. J. (2024). The future of wearable health technology: from monitoring to preventive healthcare. World J Biol Pharm Heal Sci, 20, 36-55.

[25] Hiraoka, D., Inui, T., Kawakami, E., Oya, M., Tsuji, A., Honma, K., ... & Matsumiya, G. (2022). Diagnosis of atrial fibrillation using machine learning with wearable devices after cardiac surgery: algorithm development study. JMIR Formative Research, 6(8), e35396.

[26] Guk, K., Han, G., Lim, J., Jeong, K., Kang, T., Lim, E. K., & Jung, J. (2019). Evolution of wearable devices with real-time disease monitoring for personalized healthcare. Nanomaterials, 9(6), 813.

[27] Anikwe, C. V., Nweke, H. F., Ikegwu, A. C., Egwuonwu, C. A., Onu, F. U., Alo, U. R., & Teh, Y. W. (2022). Mobile and wearable sensors for data-driven health monitoring system: State-of-the-art and future prospect. Expert Systems with Applications, 202, 117362.

[28] Mehrdad, S., Wang, Y., & Atashzar, S. F. (2021). Perspective: wearable internet of medical things for remote tracking of symptoms, prediction of health anomalies, implementation of preventative measures, and control of virus spread during the era of COVID-19. Frontiers in Robotics and AI, 8, 610653.

[29] Kaisti, M., Panula, T., Leppänen, J., Punkkinen, R., Jafari Tadi, M., Vasankari, T., ... & Pänkäälä, M. (2019). Clinical assessment of a non-invasive wearable MEMS pressure sensor array for monitoring of arterial pulse waveform, heart rate and detection of atrial fibrillation. NPJ digital medicine, 2(1), 39.

[30] Sraitih, M., Jabrane, Y., & Hajjam El Hassani, A. (2021). An automated system for ECG arrhythmia detection using machine learning techniques. Journal of Clinical Medicine, 10(22), 5450.

[31] Ullah, A., Rehman, S. U., Tu, S., Mehmood, R. M., Fawad, & Ehatisham-ul-Haq, M. (2021). A hybrid deep CNN model for abnormal arrhythmia detection based on cardiac ECG signal. Sensors, 21(3), 951.

[32] Mahmud, T., Fattah, S. A., & Saquib, M. (2020). DeepArrNet: An Efficient Deep CNN Architecture for Automatic Arrhythmia Detection and Classification From Denoised ECG Beats. IEEE Access, 8, 104788-104800.

[33] Liu, P., Sun, X., Han, Y., He, Z., Zhang, W., & Wu, C. (2022). Arrhythmia classification of LSTM autoencoder based on time series anomaly detection. Biomedical Signal Processing and Control, 71, 103228.

[34] Zeng, W., Su, B., Chen, Y., & Yuan, C. (2023). Arrhythmia detection using TQWT, CEEMD and deep CNN-LSTM neural networks with ECG signals. Multimedia Tools and Applications, 82(19), 29913-29941.

[35] Kuila, S., Dhanda, N., & Joardar, S. (2024). ECG signal classification using DEA with LSTM for arrhythmia detection. Multimedia Tools and Applications, 83(15), 45989-46016.

[36] Xu, G., Xing, G., Jiang, J., Jiang, J., & Ke, Y. (2020). Arrhythmia detection using gated recurrent unit network with ECG signals. Journal of Medical Imaging and Health Informatics, 10(3), 750-757.

[37] He, J., Rong, J., Sun, L., Wang, H., Zhang, Y., & Ma, J. (2020). A framework for cardiac arrhythmia detection from IoT-based ECGs. World Wide Web, 23(5), 2835-2850.

[38] Zhang, B., Ren, H., Huang, G., Cheng, Y., & Hu, C. (2019). Predicting blood pressure from physiological index data using the SVR algorithm. BMC bioinformatics, 20(1), 109.

[39] Rong, M., & Li, K. (2021). A multi-type features fusion neural network for blood pressure prediction based on photoplethysmography. Biomedical Signal Processing and Control, 68, 102772.

[40] Liu, L., Lu, H., Whelan, M., Chen, Y., & Ding, X. (2024). CiGNN: a causality-informed and graph neural network based framework for cuffless continuous blood pressure estimation. IEEE Journal of Biomedical and Health Informatics, 28(5), 2674-2686.

[41] Koshimizu, H., Kojima, R., Kario, K., & Okuno, Y. (2020). Prediction of blood pressure variability using deep neural networks. International Journal of Medical Informatics, 136, 104067.

[42] Ali, N. F., & Atef, M. (2023). An efficient hybrid LSTM-ANN joint classification-regression model for PPG based blood pressure monitoring. Biomedical Signal Processing and Control, 84, 104782.

[43] Zhang, B., Ren, J., Cheng, Y., Wang, B., & Wei, Z. (2019). Health data driven on continuous blood pressure prediction based on gradient boosting decision tree algorithm. Ieee Access, 7, 32423-32433.

[44] Kamanditya, B., Fuadah, Y. N., Mahardika T, N. Q., & Lim, K. M. (2024). Continuous blood pressure prediction system using Conv-LSTM network on hybrid latent features of photoplethysmogram (PPG) and electrocardiogram (ECG) signals. Scientific Reports, 14(1), 16450.

[45] Zhang, G., Choi, D., & Jung, J. (2024). Development of continuous cuffless blood pressure prediction platform using enhanced 1-D SENet–LSTM. Expert Systems with Applications, 242, 122812.

[46] Zheng Duanmu, Haojie Gong, Siyuan Lv, Wenyue Yan, Qianxi Cheng, Jinqiu Sang... & Louqian Zhang. (2025). Multi-Stage BiSTU Network Combining BiLSTM and Transformer for ABP Waveform Prediction from PPG Signals. Annals of biomedical engineering,(prepublish),1-18.

[47] Nasreddine Belbachir, Mohamed Zellagui, Haitham A. Mahmoud, Fatma A. Hashim, Radwa El Shawi, Fatma Hilal Yagin & Riyadh M. Al Tam. (2025). Optimal allocation of hybrid PVDG and DSVC devices into distribution grids using a modified NRBO algorithm considering the overcurrent protection characteristics. Scientific Reports,15(1),12871-12871.

[48] Chen Sian, Zuo Yajuan & Wang Rui. (2024). RETRACTED: An optimal framework for natural English translate processing: On the application of artificial neural network and Adam optimization algorithm. Journal of Intelligent & Fuzzy Systems,47(5-6, Supplement 1),205-219.